A model to predict the elastic field radiated by a magnetostrictive patch transducer into an omnidirectional waveguide

Guillaume Cousin, A. Lhémery, Sébastien Grondel

A model to predict the elastic field radiated by a magnetostrictive patch transducer into an omnidirectional waveguide

G Cousin[1,2], A Lhémery[1] and S Grondel[2]

[1] Université Paris-Saclay, CEA LIST, F-91191, Gif-sur-Yvette, France
[2] UPHF, F-59313, Valenciennes, France

E-mail: alain.lhemery@cea.fr

Abstract. Magnetostrictive patch transducers (MPT) can be used as sources or sensors of elastic guided waves in non-destructive testing and structural health monitoring methods. A tool for simulating them is under development to help designing optimal MPT for a given application. It requires the prior accurate modelling of transduction phenomena involved in such patches and of the GW fields they generate. A MPT is made of a thin magnetostrictive strip under a static magnetic field, glued to the waveguide under examination and excited by an alternative current circulating in a coil. In the strip where they take place, transduction phenomena are similar to those generated by an electro-magnetic acoustic transducer (EMAT) in a ferromagnetic medium. They involve magnetostrictive strain, magnetization force and surface traction and Lorentz force (Clausse *et al.* 2017 *J. Phys.: Conf. Ser.* **797** 102004), which can be transformed into equivalent surface stresses at the outer surface of the strip. A matrix model is developed to propagate the equivalent stresses from this outer surface to that of the waveguide. Once equivalent stress distributions are computed at this latter surface, a model (Barras *et al.* 2020 *Ultrasonics* **103** 1060782) is used to predict the MPT radiation into the waveguide. Overall, the chaining of these models constitutes a semi-analytical multi-physics model for GW radiation by MPT of high computing efficiency.

1. Introduction

In guided wave (GW) nondestructive testing (NDT) methods or structural health monitoring (SHM) methods, elastic waves are generated by one or several sources into a waveguide under examination, propagate and possibly interact with flaws and are received by one or several sensors. Various sources and sensors can be used such as electromagnetic acoustic transducer (EMAT), piezoelectric transducers or magnetostrictive patch transducers (MPT), depending on specific requirements relative to cases to handle. The scientific literature on these subjects together with the industrial use of such techniques describe all sort of arrangements of sources and sensors, possibly of different kinds for the radiation and for the reception (see reference [1] for a review on GW SHM).

Phenomena related to GW radiation, propagation, scattering and reception, are complex. Simulation able to handle such complexity is a very helpful tool to ease the design of optimal NDT/SHM methods and to accurately interpret experimental results. To be fully operational, a simulation tool must not only handle the complexity, but also be both accurate and computationally efficient enough to be used intensively. At CEA, the development of such simulation tools for various NDT/SHM techniques has been the subject of researches for decades for developing models, for implementing and validating them

and subject of software developments (the CIVA simulation platform; see [2] for modules relative to methods involving GW) to make these tools usable by NDT engineers and technicians.

Piezoelectric as well as EMAT transducers are currently modelled in CIVA. For EMAT, the current (commercially available) version of CIVA deals with nonmagnetic materials. However, a model of EMAT generating elastic waves in ferromagnetic media has been developed, validated [3, 4] and implemented in a laboratory version of CIVA. This model accounts for the various electro-magneto-elastic phenomena that can lead to the excitation of elastic waves at ultrasonic frequency. These include Lorentz force, which takes place in any conducting medium, as well as dynamic magnetoelastic effects that take place only in magnetic media: magnetostrictive strain, magnetization force (to be treated together with Lorentz force [5]) and surface traction term related to magnetic field discontinuity at the surface of the ferromagnetic material [5]. The various bulk source terms can be transformed into equivalent surface stresses where the EMAT operates using a mathematical transformation detailed in [6], which is valid as long as bulk sources are at short distance of the surface, that is, at depths far shorter than the shortest wavelength of radiated elastic waves.

Magnetostrictive patch transducers (MPT) share many similarities with EMAT [7]. MPT are made of a thin strip of highly magnetostrictive material (such as Nickel, Fe-Co), which is pre-magnetized or magnetized by a permanent magnet or an electromagnet, and an electrical circuit (a coil) in which a HF current is injected. Transduction phenomena arise in a thin layer of the magnetostrictive strip rather than at the surface of the piece under examination when an EMAT is used. The thin strip is generally glued to the piece under examination. MPT can be very useful and are actually used in many SHM and generally speaking NDT configurations [7]. They constitute an effective alternative to piezoelectric transducers. Specifically, they can be designed to offer high modal selectivity in GW radiation.

The present paper aims at developing a model for predicting the GW field radiated by an arbitrary MPT. Specifically, we want to adapt the model for EMAT radiation in ferromagnetic media [3, 4] to model the patch behavior. Moreover, as MPT are mostly used in the context of methods involving GW, the MPT model to be developed must be easily adapted to different models developed at CEA for predicting GW field radiation, which assume sources described as distributions of surface stresses [8, 9].

In the first part of the present paper (Sec. 2 Theory), we want to i) show how the model of EMAT radiation into ferromagnetic media can be used to predict the dynamic sources generated in a patch, ii) study how these sources are modified by the multilayered structure of a patch glued to a waveguide, iii) find a way to describe the effective sources generated at the guide surface as distributions of equivalent surface stresses. It is shown that effective sources of surface stresses can be obtained semi-analytically using Thomson-Haskell [10, 11] approach of propagation in multilayered media. In the second part (Sec. 3, Validation), the semi-analytical model of equivalent sources is validated by comparing its predictions to results computed by an in-house finite-element code solving the time-dependent equation of elastodynamics [9]. Starting with a simple 1D case, we progressively consider more complex cases up to a realistic 3D MPT configuration. In the third part (Sec. 4, Application to a realistic MPT configuration), the MPT model is used to compute sources to be inputted in a recently developed model allowing the modal computation of GW radiated by arbitrary sources in a plate [8]. This demonstrates how an adequately designed MPT can be a highly selective source of one chosen mode among all the modes existing in the frequency range considered.

2. Theory
2.1. Operational principle of a magnetostrictive patch transducer

A magnetostrictive patch transducer (MPT) is made of two distinct elements: i) a ferromagnetic highly magnetostrictive thin strip (Ni, Fe-Co alloy) that is either glued to the part to be examined (in what follow, the waveguide) or in dry contact with it [7]. ii) a conductive wire, in which a HF time-dependent current is injected, which can be given various shapes as this is done for the electric circuit of an EMAT. The magnetostrictive strip is generally magnetized (static bias field): it is either pre-magnetized with a permanent magnet once the strip has been glued to the guide and before the electrical circuit is added, or magnetized by a permanent magnet and an electromagnet while in use.

As already pointed out in the introduction, transduction mechanisms of a MPT, in overall, are similar to those of an EMAT radiating in a ferromagnetic medium. More specifically, the same electro-magneto-elastic phenomena operate, all being local effects resulting from the generation of dynamic currents in a conductive magnetic and elastic medium under a static magnetic field as described in [3, 4]. The main difference is that these phenomena are induced by an EMAT in the piece itself, whereas they are induced in the magnetostrictive strip – a ferromagnetic medium – in the case of a MPT. In other words, the same transduction phenomena take place, leading to dynamic elastic sources directly in the piece where waves must propagate for its examination in the former case, but still external to the piece in the latter case.

The various phenomena can be of highly differing amplitudes depending on the frequency range of the excitation current circulating in the electrical circuit, on the conductivity and magnetic properties of the material where they are induced, on its magneto-elastic characteristics, but also depending on the geometrical arrangement of the wire (spiral, meander-coil, series of straight parallel wires etc) and on the characteristics of the static magnetic field (intensity, spatial distribution). As far as our contribution to the modelling of MPT is concerned, we entirely rely on the model developed in [3, 4] of EMAT radiation in ferromagnetic media. Only dynamic phenomena are taken into account as these are the only phenomena that are sources of elastic waves. They arise in the region of the ferromagnetic medium where the electro-magnetic field induced by the current circulating in the wire(s) is at its highest. This region is situated essentially below the trace of the wires at the surface of the ferromagnetic medium and extends over a depth that can be given as a few times the value of the skin depth.

The skin depth $\delta_p = (\pi\mu_0\mu_r\sigma f)^{-1/2}$, a frequency-dependent distance, is the depth above which the induced field is higher than $1/e$ times the highest amplitude (at the surface itself). In the expression of skin-depth, μ_0 is the permeability of vacuum ($4\pi\ 10^{-7}\ H.m^{-1}$), μ_r is the relative permeability of the material considered, σ is the conductivity and f is the frequency. Let us consider a strip made of pure Ni with a relative permeability of 600 and a conductivity of $14.3 \times 10^6 S.m^{-1}$. At a frequency of 100 kHz the skin depth equals 21.5 μm. This means that at a depth of about $100\mu m$, the amplitude is less than 1% of the value at the surface due to its exponential decrease and transduction phenomena become almost negligible. So, the bulk transduction phenomena actually arise in a very thin layer below the surface of the ferromagnetic medium. It has been shown [4, 6] that, as long as bulk sources are at depths much shorter than the wavelength of the generated elastic wave, it is possible mathematically to transform them into equivalent surface sources of stress (readers interested in details about this transformation are referred to [6]).

At this stage, the model for EMAT radiation in ferromagnetic media [3, 4] is used to predict the various electro-magneto elastic sources (bulk dynamic magnetization and Lorentz forces to be predicted together with dynamic magnetic surface traction and bulk magnetostriction strain). These sources depend on magnetization and magnetostriction curves specific of the material considered. These curves can be either measured or predicted. Here, Daniel's theory [13] is used to predict them. These predictions are made within CIVA module dedicated to eddy-current testing simulation, allowing easy computation of the electromagnetic static and dynamic fields involved in the EMAT source model, for arbitrary geometry of coil, arbitrary permanent magnet. From these electromagnetic static and dynamic fields, the bulk elastodynamic source are predicted [4]. Once these sources have been computed, they are transformed into equivalent sources of surface stress at the upper surface of the patch [6].

It is now necessary to study what this source of surface stress generates at the surface of the waveguide through the magnetostrictive strip and the glue layer.

2.2. Transferring dynamic stresses from the top of the magnetostrictive strip to the guide surface
The so-called Thomson-Haskell (TH) method was initially developed by Thomson [10], then slightly modified by Haskell [11]. This method enables to link a state-vector from one plane of a multi-layered medium of infinite extent to another such plane through the use of a transfer matrix to be computed. Its application is sometimes challenging due to possible bad conditioning of the matrix but many alternative methods (starting with [12]) were proposed to overcome these difficulties when required.

A MPT coupled to a planar guide can be modelled as a 3-layer-medium: the magnetostrictive strip, the glue layer and the waveguide, as shown on Fig. 1. In the present case of three layers with two thin ones (magnetostrictive strip and glue), the TH method is suitable to predict plane wave behaviour everywhere in this structure.
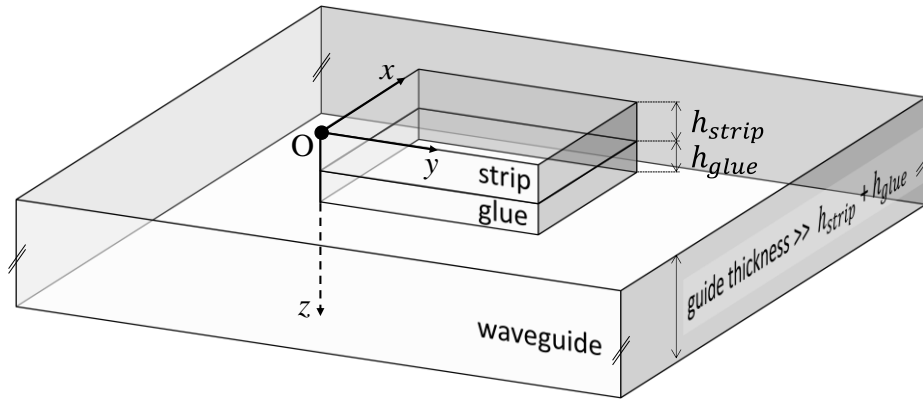

Figure 1. A MPT glued to a waveguide modelled as a 3-layer medium with perfect contact between two neighbouring layers.

At the top free surface of the magnetostrictive strip, the source of equivalent surface stress has been computed as described in the previous subsection.

The transfer matrix formulation relies on one mathematical ingredient and one assumption on continuity properties at the parallel interfaces between the various layers. The mathematical ingredient is the possibility to decompose, thanks to Fourier transformations, an arbitrary wave field in a multi-layered medium (here, parallel horizontal isotropic layers) into imbricated sums of harmonic plane elastic waves of elementary polarizations (transverse vertical or transverse horizontal and longitudinal). The assumption made on interface properties is that they are all considered as perfect solid-solid contact interfaces, leading to continuity of particle displacement and stress. By combining this ingredient and this assumption, a given incident plane wave of wavenumber $\vec{k}$ (k_x, k_y, k_z) will be reflected, transmitted and mode converted into a series of plane waves having the same horizontal wavenumber components (k_x, k_y). This simply results from Snell-Descartes law at interfaces.

2.2.1. Plane wave decomposition of particle displacement. Let $\vec{z}$ denotes the normal to the top surface of the waveguide. A wavefield can be decomposed in the spatial frequency and time frequency domain as sums of continuous plane waves. One possible decomposition is given by (*e.g.*, field of particle displacement $\boldsymbol{u}$):

$$\boldsymbol{u}(t,x,y) = \int_\omega \int_{k_x} \int_{k_y} \hat{\boldsymbol{u}}(\omega, k_x, k_y) e^{i(\omega t - k_x x - k_y y)} \, d\omega \, dk_x dk_y \tag{1}$$

where the double spatial Fourier transform was calculated in a plane parallel to the guide top surface. Properties of plane elastic wave at oblique incidence on a planar interface between two isotropic media in perfect solid-solid contact are used. The wavefield is decomposed into waves of longitudinal (P) transverse vertical (SV) and transverse horizontal (SH) polarities, propagating upward (-) or downward (+). The projection on a planar interface of the wavenumber $\vec{k}$ of transmitted and reflected waves is identical to that of the incident wave. The particle displacement can be written as a sum of six waves as

$$\hat{\boldsymbol{u}}(\omega, k_x, k_y) = \hat{\boldsymbol{u}}_P^+ + \hat{\boldsymbol{u}}_P^- + \hat{\boldsymbol{u}}_{SV}^+ + \hat{\boldsymbol{u}}_{SV}^- + \hat{\boldsymbol{u}}_{SH}^+ + \hat{\boldsymbol{u}}_{SH}^-. \tag{2}$$

The various contributions in Eq. (2) are now written in more detailed as:

$$\hat{\boldsymbol{u}}_P^{\pm} = A_P^{\pm} \frac{\left(k_x, k_y, \pm k_z^P\right)^t}{\left\|\left(k_x, k_y, \pm k_z^P\right)^t\right\|} e^{i\left(\omega t - \overrightarrow{k_P^{\pm}} \cdot \vec{r}\right)}, \tag{3}$$

$$\hat{\boldsymbol{u}}_{SV}^{\pm} = A_{SV}^{\pm} \frac{\left(\pm k_x k_z^S, \pm k_y k_z^S, -\left(k_x^2 + k_y^2\right)\right)^t}{\left\|\left(\pm k_x k_z^S, \pm k_y k_z^S, -\left(k_x^2 + k_y^2\right)\right)^t\right\|} e^{i\left(\omega t - \overrightarrow{k_S^{\pm}} \cdot \vec{r}\right)}, \tag{4}$$

$$\hat{\boldsymbol{u}}_{SH}^{\pm} = A_{SH}^{\pm} \frac{\left(k_y, -k_x, 0\right)^t}{\left\|\left(k_y, -k_x, 0\right)^t\right\|} e^{i\left(\omega t - \overrightarrow{k_S^{\pm}} \cdot \vec{r}\right)}, \tag{5}$$

where $A_{P,SV,SH}^{\pm}$ denote the amplitudes of waves propagating upward or downward with the three possible polarizations, with $\vec{k}_P^{\pm} = \left(k_x, k_y, \pm k_z^P\right)$, with $k_z^P = \left(\omega^2/v_P^2 - k_x^2 - k_y^2\right)^{1/2}$ that requires $Im(k_z^P) \leq 0$ and with $\vec{k}_S^{\pm} = \left(k_x, k_y, \pm k_z^S\right)$ and $k_z^S = \left(\omega^2/v_S^2 - k_x^2 - k_y^2\right)^{1/2}$ that requires $Im(k_z^S) \leq 0$, and where $\vec{r} = (x, y, z)^t$ is the position vector inside a homogeneous layer.

2.2.2. *State vector and propagation in a single medium.* The overall aim of Sec. 2.2. is to study the elastodynamic transfer of a known source at the top MPT surface to the guide surface. For this, it is necessary to express the elastic wave field anywhere in the multilayered medium by taking into account boundary conditions between layers. Since these conditions involve writing continuity equations for both particle displacement $\hat{\boldsymbol{u}} = \left(\hat{u}_x, \hat{u}_y, \hat{u}_z\right)^t$ and stress components $\hat{\boldsymbol{\sigma}} = \left(\hat{\sigma}_{xz}, \hat{\sigma}_{yz}, \hat{\sigma}_{zz}\right)^t$ (assuming perfect solid-solid contact at the interface between two layers), it is necessary to take together into account all these elastodynamic quantities.

In what follows, the state vector $(\hat{\boldsymbol{u}} \quad \hat{\boldsymbol{\sigma}})^t = \left(\hat{u}_x, \hat{u}_y, \hat{u}_z, \hat{\sigma}_{xz}, \hat{\sigma}_{yz}, \hat{\sigma}_{zz}\right)^t$ is considered. Stress and displacement components are assumed to be linked by linear relations (Hooke's law). Explicit use of Hooke's law applied to the displacement decomposed as made in Eq. (2) allows us to write the state vector at a given plane z_2 as a function of wave amplitudes at a plane z_1. Note that the full demonstration of expressions that follow (including matrix expression appearing in Appendix A) is not given herein by lack of place. It is possible to show that these general 3D expressions simplify into Thomson-Haskell expressions when considering only 2D cases as initially derived in their papers. One can formally write the state vector at z_2 as

$$\binom{\hat{\boldsymbol{u}}}{\hat{\boldsymbol{\sigma}}}(z_2) = D_m(z_2 - z_1)\boldsymbol{A}(z_1), \tag{6}$$

where $\boldsymbol{A} = (A_P^+ \ A_P^- \ A_{SV}^+ \ A_{SV}^- \ A_{SH}^+ \ A_{SH}^-)^t$. The subscript "$m$" refers to the material of a given layer, its elastic characteristics being taken into account when expressing matrix D_m given in Appendix A.

Now, the matrix E_m^{-1} is built so that $E_m = D_m(0)$. It enables to write:

$$\boldsymbol{A}(z_1 = z_2) = E_m^{-1}\binom{\hat{\boldsymbol{u}}}{\hat{\boldsymbol{\sigma}}}(z_2 = z_1). \tag{7}$$

By combining Eqs. (6) and (7), one gets:

$$\binom{\hat{\boldsymbol{u}}}{\hat{\boldsymbol{\sigma}}}(z_2) = L_m(z_2 - z_1)\binom{\hat{\boldsymbol{u}}}{\hat{\boldsymbol{\sigma}}}(z_1), \tag{8}$$

where $L_m(z_2 - z_1) = D_m(z_2 - z_1) \cdot E_m^{-1}$.

2.2.3. Propagation through different media. We can now express a matrix linking the two interfaces of interest for modelling the propagation into the patch (magnetostrictive strip and glue layer), namely, the top surface of the patch and the top surface of the waveguide. For this, Eq. (8) is used to express the state vector at the various interfaces of the multi-layered medium. For the magnetostrictive strip of height h_{strip} one has:

$$\begin{pmatrix} \widehat{\boldsymbol{u}} \\ \widehat{\boldsymbol{\sigma}} \end{pmatrix}(h_{strip}) = L_{strip}(h_{strip}) \begin{pmatrix} \widehat{\boldsymbol{u}} \\ \widehat{\boldsymbol{\sigma}} \end{pmatrix}(0), \tag{9}$$

reference $z = 0$ being the top surface of the strip, as shown on Fig. 1. For the glue layer of height h_{glue}, one has:

$$\begin{pmatrix} \widehat{\boldsymbol{u}} \\ \widehat{\boldsymbol{\sigma}} \end{pmatrix}(h_{strip} + h_{glue}) = L_{glue}(h_{glue}) \begin{pmatrix} \widehat{\boldsymbol{u}} \\ \widehat{\boldsymbol{\sigma}} \end{pmatrix}(h_{strip}). \tag{10}$$

By combining Eqs. (9) and (10), one gets:

$$\begin{pmatrix} \widehat{\boldsymbol{u}} \\ \widehat{\boldsymbol{\sigma}} \end{pmatrix}(h_{strip} + h_{glue}) = L_{glue}(h_{glue})L_{strip}(h_{strip}) \begin{pmatrix} \widehat{\boldsymbol{u}} \\ \widehat{\boldsymbol{\sigma}} \end{pmatrix}(0). \tag{11}$$

Equation (11) enables computing the state-vector at the waveguide surface from that at the patch top surface. The latter is however not fully determined at this stage, only stresses (here, the source of stress) being known. To compute the displacement at the surface of the patch, a boundary condition must be introduced that concerns the way waves propagate in the elastic waveguide.

2.2.4. Boundary condition for the waveguide: the infinite half-space. The input of the model is the stress $\widehat{\boldsymbol{\sigma}}$ at $z = 0$ while the particle displacement is unknown. To solve Eq. (11), supplementary conditions must be introduced. The possibility of momentarily considering that the waveguide (this being of finite thickness by definition) behaves as a half space has been studied. The thicknesses of the strip and of the glue layer are small compared with the thickness of typical waveguides to be considered in practice. In terms of wave contributions, considering the waveguide as being semi-infinite consists in saying that there exists no wave propagating upward (-) in the guide medium. Clearly, this means that the actual coupling of the MPT to the guide is not fully taken into account: it is assumed that waves generated in the guide cannot influence the MPT behaviour. Note that this assumption is almost always made, whatever the nature of the source to be modelled. It is the only way of predicting a complex transduction process independently of the geometry of the piece where the wavefield is studied. On the other hand, elastic characteristics of the piece are taken into account as the downward wave propagation in the piece medium is explicitly taken into account.

By combining Eqs. (7) and (11) and by applying Eq. (7) to the waveguide, wave amplitudes at the surface of the guide writes:

$$\boldsymbol{A}(h_{strip} + h_{glue}) = E_{waveguide}^{-1} L_{glue}(h_{glue}) L_{strip}(h_{strip}) \begin{pmatrix} \widehat{\boldsymbol{u}} \\ \widehat{\boldsymbol{\sigma}} \end{pmatrix}(0). \tag{12}$$

Let H^{SI} denote the product of matrices expressed as $H^{SI} = E_{waveguide}^{-1} L_{glue}(h_{glue}) L_{strip}(h_{strip})$. We now introduce the effect of the boundary condition discussed above by specifying that the amplitudes of waves in the guide propagating upward are set equal to zero at the MPT – guide interface (at $z = h_{strip} + h_{glue}$). Therefore, Eq. (12) can be formally rewritten as:

$$
\begin{pmatrix} A_P^- = 0 \\ A_{SV}^- = 0 \\ A_{SH}^- = 0 \end{pmatrix} = \begin{bmatrix} H_{21}^{SI} & H_{22}^{SI} & H_{23}^{SI} & H_{24}^{SI} & H_{25}^{SI} & H_{26}^{SI} \\ H_{41}^{SI} & H_{42}^{SI} & H_{43}^{SI} & H_{44}^{SI} & H_{45}^{SI} & H_{46}^{SI} \\ H_{61}^{SI} & H_{62}^{SI} & H_{63}^{SI} & H_{64}^{SI} & H_{65}^{SI} & H_{66}^{SI} \end{bmatrix} \begin{pmatrix} \widehat{\boldsymbol{u}} \\ \widehat{\boldsymbol{\sigma}} \end{pmatrix}(0). \tag{13}
$$

From Eq. (13), it is possible to express the particle displacement at the top surface of the patch ($z = 0$):

$$
\begin{pmatrix} \hat{u}_x \\ \hat{u}_y \\ \hat{u}_z \end{pmatrix}(z = 0) = - \begin{bmatrix} H_{21}^{SI} & H_{22}^{SI} & H_{23}^{SI} \\ H_{41}^{SI} & H_{42}^{SI} & H_{43}^{SI} \\ H_{61}^{SI} & H_{62}^{SI} & H_{63}^{SI} \end{bmatrix}^{-1} \begin{bmatrix} H_{24}^{SI} & H_{25}^{SI} & H_{26}^{SI} \\ H_{44}^{SI} & H_{45}^{SI} & H_{46}^{SI} \\ H_{64}^{SI} & H_{65}^{SI} & H_{66}^{SI} \end{bmatrix} \begin{pmatrix} \hat{\sigma}_{xz} \\ \hat{\sigma}_{yz} \\ \hat{\sigma}_{zz} \end{pmatrix}(z = 0). \tag{14}
$$

Thanks to Eq. (14), the state-vector at this surface is now complete. Equation (11) can further be computed to get the state-vector at the surface of the waveguide. The transfer from the top surface of the patch to the top surface of the waveguide is thus expressed the most general way by combining Eqs. (14) and (11).

Note that in the literature, contributions of SH plane-waves and those of SV and P plane-waves are generally treated as two bi-dimensional independent problems. Here, all the contributions were treated within the same matrix formulation. However, in the special case of a vertical wave motion (when $k_x = k_y = 0$), matrix E cannot be built properly. A specific treatment of this particular case is given hereafter.

2.2.5. Transfer matrix for vertical wave motion. This special case arises for a uniform source of stress, corresponding to a purely 1D problem. It must be solved a different way. The particle displacement in the special case is readily given by:

$$
u_x = k_z^S \left(A_{S_j}^+ e^{i(\omega t - k_z^S z)} - A_{S_j}^- e^{i(\omega t + k_z^S z)} \right), j = x \text{ or } y, \tag{15a}
$$

$$
u_z = k_z^P \left(A_P^+ e^{i(\omega t - k_z^P z)} - A_P^- e^{i(\omega t + k_z^P z)} \right). \tag{15b}
$$

Equation for stress is determined using Eqs. (15) and Hooke's law. One gets

$$
\begin{pmatrix} u_i \\ \sigma_{iz} \end{pmatrix}(z_2) = D_{m,S}^0(z_2 - z_1) \begin{pmatrix} A_{S_i}^+ \\ A_{S_i}^- \end{pmatrix}(z_1), i = x \text{ or } y \tag{16a}
$$

$$
\begin{pmatrix} u_z \\ \sigma_{zz} \end{pmatrix}(z_2) = D_{m,P}^0(z_2 - z_1) \begin{pmatrix} A_P^+ \\ A_P^- \end{pmatrix}(z_1), \tag{16b}
$$

$$
\begin{pmatrix} A_{S_i}^+ \\ A_{S_i}^- \end{pmatrix}(z_2 = z_1) = \left[E_{m,S}^0 \right]^{-1} \begin{pmatrix} u_i \\ \sigma_{iz} \end{pmatrix}(z_1 = z_2), i = x \text{ or } y \tag{17a}
$$

$$
\begin{pmatrix} A_P^+ \\ A_P^- \end{pmatrix}(z_2 = z_1) = \left[E_{m,P}^0 \right]^{-1} \begin{pmatrix} u_z \\ \sigma_{zz} \end{pmatrix}(z_1 = z_2), \tag{17b}
$$

$$
\begin{pmatrix} u_i \\ \sigma_{iz} \end{pmatrix}(z_2) = L_{m,S}^0(z_2 - z_1) \begin{pmatrix} u_i \\ \sigma_{iz} \end{pmatrix}(z_1), i = x \text{ or } y \tag{18a}
$$

$$
\begin{pmatrix} u_z \\ \sigma_{zz} \end{pmatrix}(z_2) = L_{m,P}^0(z_2 - z_1) \begin{pmatrix} u_z \\ \sigma_{zz} \end{pmatrix}(z_1). \tag{18b}
$$

with $L_{m,S}^0(z_2 - z_1) = D_{m,S}^0(z_2 - z_1)\left[E_{m,S}^0\right]^{-1}$ and $L_{m,P}^0(z_2 - z_1) = D_{m,P}^0(z_2 - z_1)\left[E_{m,P}^0\right]^{-1}$. Matrices appear with a superscript "0" added to differentiate them from those appearing in the general case. Their (simplified) expressions are also given in Appendix A.

Then, the same steps as those in subsections 2.2.3. and 2.2.4. can be followed straightforwardly to obtain the complete state vector at the guide surface as a function of the state vector at the patch surface.

2.2.6. Summary. The matrix model developed in Sec. 2.2. allows us to deal with any component of plane elastic wave propagating from the source surface (top surface of the patch) to the surface of the guide, and to quantitatively specify the amplitude of stress at the surface of the guide. The propagation through the strip and glue layers implicitly includes phenomena of multiple reflections on and transmissions through the various interfaces. The use of real-valued stiffness constants leads to straightforward verification of energy conservation, but the use of complex-valued constants is also possible to model energy lost due to viscoelasticity in the glue for example. All these wave phenomena result in spatial filtering effects so that the equivalent stress distributions resulting from transduction phenomena in the magnetostrictive strip and the stress distributions at the surface of the guide will differ. In the model, an assumption has been made that the guide has the same effect on patch behaviour as a semi-infinite medium of identical elastic characteristics. Under this assumption, stress distributions at the guide surface predicted by the present model, once computed for one given guide material, can be reused when dealing with other guides made of the same material. Next section show how the present model, based upon plane wave decomposition followed by a matrix formulation, is quantitatively accurate by comparing its predictions to predictions computed using a finite element code developed at CEA [9].

3. Validations

To validate the model presented in Sec. 2, results predicted using this approach are compared to results predicted using an in-house time-dependent finite element code [9]. The validation is performed by considering three cases of increasing complexity. The first case is that of a uniform normal stress distribution, a 1D problem. The second case considers a 2D spatially periodical distribution of stress. The last case is that of a synthetic source of stresses mimicking that generated by a meander coil in a patch, a full 3D problem. In all three cases, a 0.2-mm-thick magnetostrictive strip made of pure nickel is considered. It is glued to a waveguide through a 0.2-mm-thick glue (epoxy) layer. The waveguide is a 5-mm-thick plate made of steel. Elastic characteristics of the various media are given in Table 1. In each case modelled by FEM, the steel part is surrounded by perfectly matched layers to ensure that no upward waves arises from the bottom of the steel plate.

Table 1. Elastic constant and thickness of layers use to model the MPT

	λ (GPa)	μ (GPa)	ρ $(kg.dm^{-3})$	h (mm)
Nickel	136.4	83.6	8.9	0.20
Epoxy	1.27	0.597	1.17	0.20
Steel	146	75.2	7.85	−

3.1. Uniform source (1D)

In the simple case of a uniform distribution of normal stress, the wavenumber associated with this source is unique and along the normal direction ($k_x = k_y = 0$). The time dependency of the stress source considered in the computations as shown by Fig. 2 (left) is a sine function of 200 kHz weighted by a Hann window. As the distribution of stress is uniform at the top of the MPT, that at the top surface of the waveguide is uniform too (1D problem). Figure 2 (right) shows the time dependency of stress computed by the present model and the FE model.

The two signals superimpose perfectly. It can be concluded that in the simple case of uniform source, the present approach is valid.
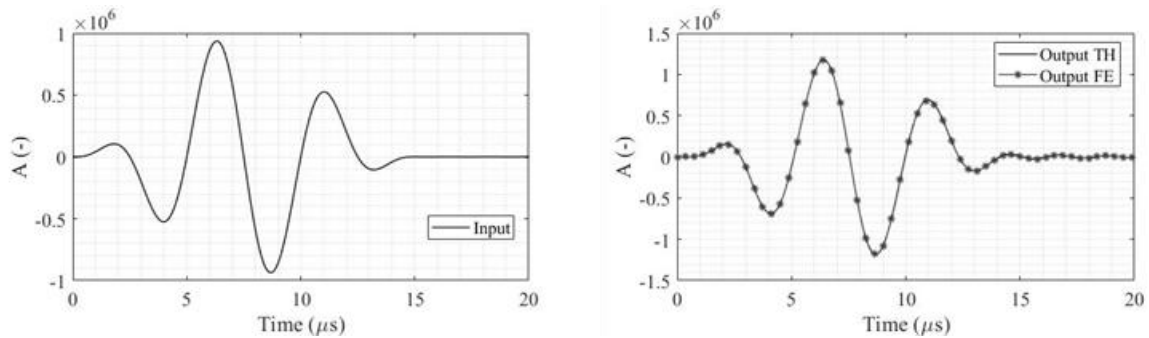
Figure 2. Time-dependencies of stress at the top of the MPT (left) and at the surface of the guide (right).

Two remarks can be made at this stage: 1) in the computation, the energy is conserved, as stiffness constants are real-valued. The stress amplitude is different at the two surfaces, as predicted by both models. Here, it is higher at the piece surface than at the top surface of the patch. At the same time, the amplitude of the particle velocity decreases. Even if the thicknesses of the magnetostrictive strip and of the glue layer are far smaller than the wavelength of plane-waves involved (2.4 *mm* for a *P* plane-wave at 200 *kHz* in nickel, 1.2 *mm* for a *P* plane-wave at 200 *kHz* in epoxy), the propagation through these layers must be carefully taken into account for the quantitative prediction of wave generation by a MPT. 2) In the present case, a (1D) normal stress is considered, thus only a longitudinal wave is generated. It propagates at $4500 m.s^{-1}$ in the magnetostrictive strip and at $1450 m.s^{-1}$ in the glue layer, resulting in a $0.18 \mu s$ time delay between the two surfaces. Such a delay is hardly visible in Fig. 2 (between the top surface on left and the guide surface on right).

3.2. Periodical source (2D)
The second case of validation is that of a source defined as a spatially periodical distribution of tangential stress with a spatial period denoted by λ, as shown on Fig. 3. Such a source generates shear horizontal (SH) modes in a plate.
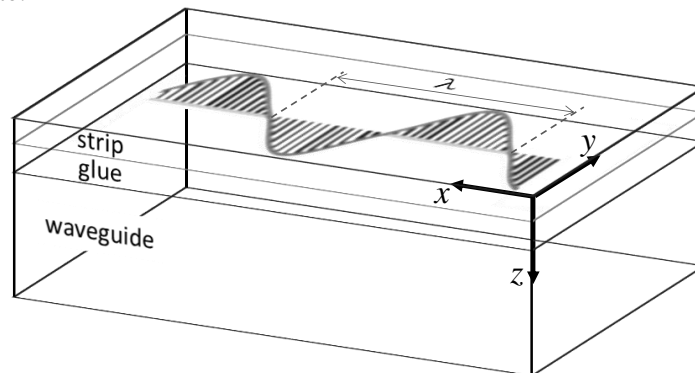

Figure 3. Schematic view of a spatially periodical source of σ_{yz} at the top surface of a MPT.

Figure 4 (left) shows the time-dependency of horizontal stress applied at the top surface of the strip (a sine function of 50 *kHz* weighted by a Hann window). Figure 4 (right) shows the time dependency of the horizontal stress predicted by both the present model and by FE, at the surface of the waveguide, the source parameter λ being equal to 20 *mm*. Again, the two predicted waveforms perfectly superimpose. Note that in the present case, the amplitude at the surface of the waveguide is lower than that at the top surface of the magnetostrictive strip, proving how these variations are highly dependent on the configuration considered.
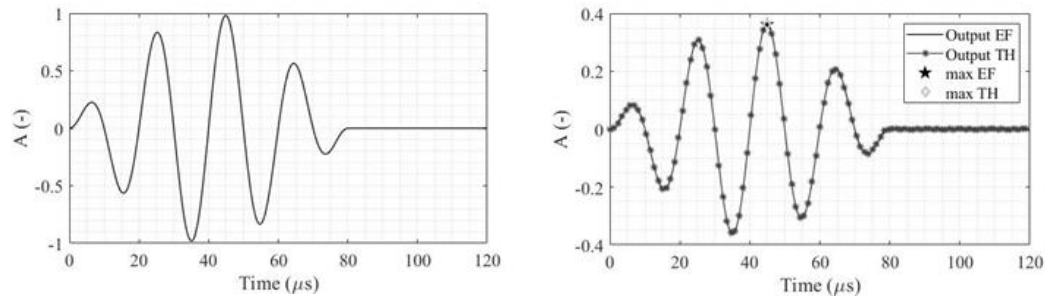
Figure 4. Time-dependency of the tangential stress at top surfaces of the strip (left), the guide (right).

To go further, a parametric study is carried out to show the influence of the source period onto the maximum amplitude of tangential stress transmitted at the top surface of the guide. This parametric study is easy to carry out with the present model as it is semi-analytical, whereas precautions must be taken in the FE computations so that the mesh of propagative media is perfectly adapted to the different sources considered (of varying size).
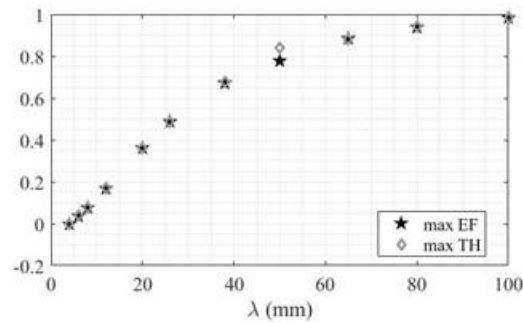The amplitude is extracted from the full waveforms predicted by both models (Fig. 5).

Figure 5. Maximum amplitude of waveforms predicted by the present
model and by FE for an excitation centre-frequency of 50 *kHz*.

Whatever the value of parameter λ, both models are in excellent agreement. These results constitute a supplementary proof of the validity of the present model. It is important to note that the patch configuration operates a low-pass filtering of wavenumbers (higher amplitude of waves of longer wavelength).

3.3. Meander-coil-like source (3D)
The last type of source used for the numerical validation is a meander-coil-like source, On Fig. 6, the three distributions of surface stresses that are the inputs of present simulations are displayed at the same amplitude scale. The interest of considering a synthetic source of simple definition (components of tangential stress parallel to the wires and of constant value and some normal stress at corners) is that it can be accurately defined on a FE mesh.
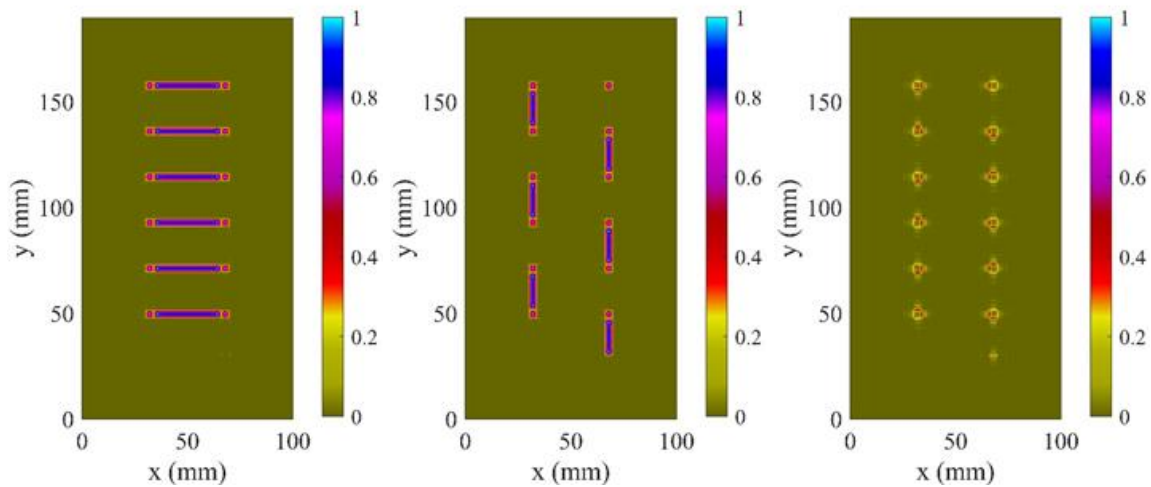
Figure 6. Equivalent stress distributions at the top surface of the magnetostrictive strip, computed by mean of source models [3-5]. From left to right: $\sigma_{xz}, \sigma_{yz}, \sigma_{zz}$

The outputs of both models are shown as maximum amplitude maps (absolute values) for the three components of surface stress at the guide surface. Figure 7 (resp. 8) shows the distributions computed using the present model (resp. FE model) at the surface of the waveguide.

Results are in excellent agreement for all the component of the stress. Compared to the source of stresses shown in Fig. 6, stresses at the guide surface are smoothed by the propagation through the strip and glue layers.
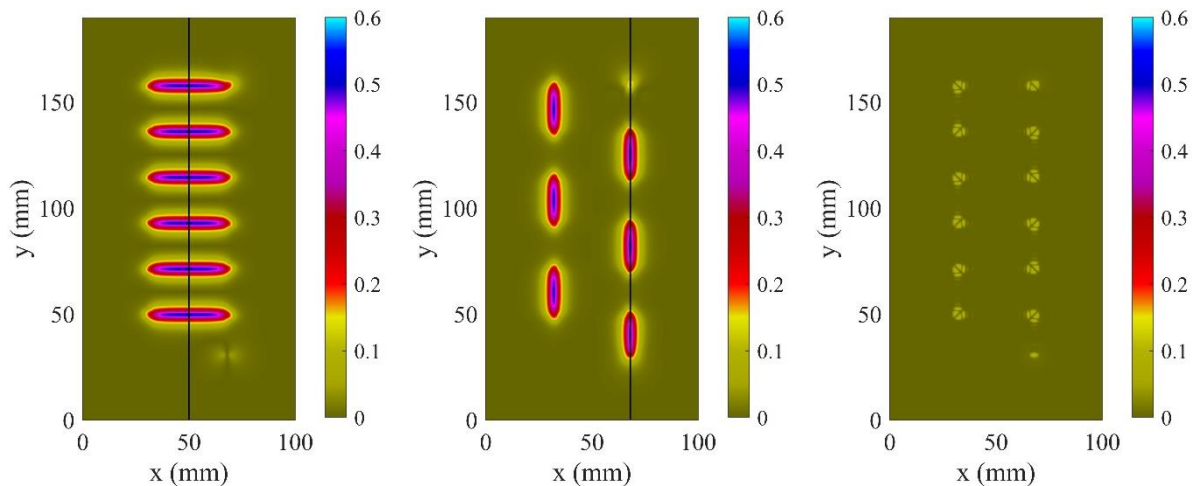

Figure 7. Stress distributions on the guide surface using the present approach.
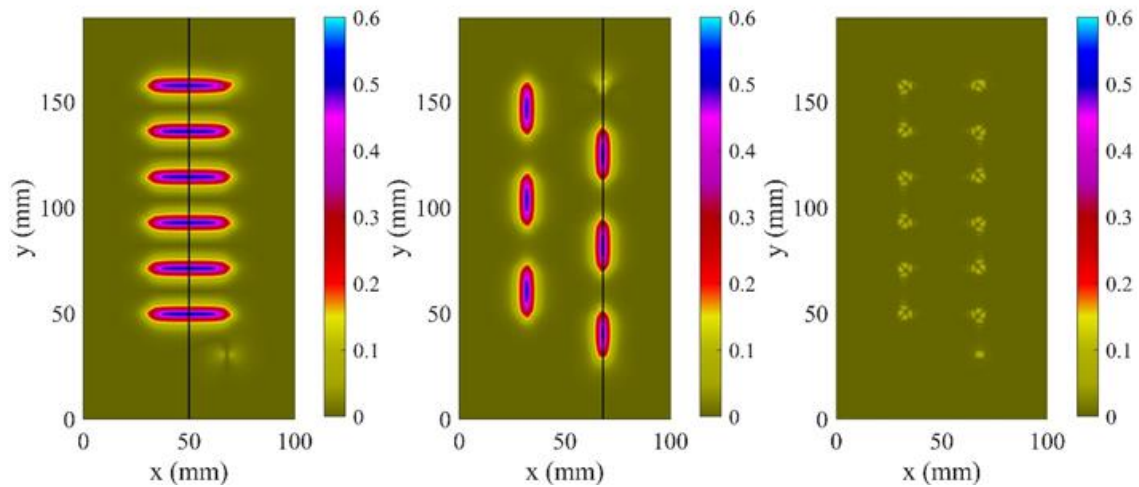From left to right: $\sigma_{xz}, \sigma_{yz}, \sigma_{zz}$

Figure 8. Stress distributions on guide surface using FE computation.
From left to right: $\sigma_{xz}, \sigma_{yz}, \sigma_{zz}$

From previous results, amplitudes are extracted for points of the maps along the two vertical lines appearing on σ_{xz} and σ_{yz} results and superimposed (Fig. 9), allowing easier quantitative comparison.
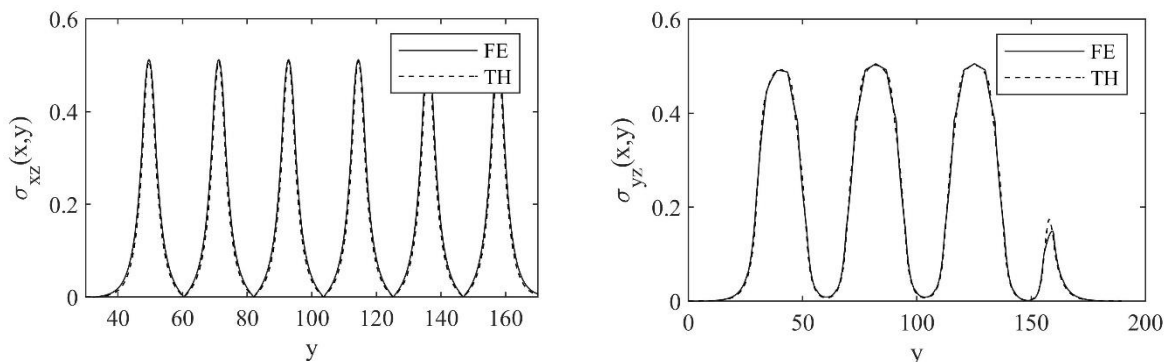

Figure 9. Superimposition of stress results computed by the present model (TH) and by FE for points taken on lines shown in previous figures. Left: σ_{xz}. Right: σ_{yz}.

Again, results given with this example show that the multi-layered structure of a MPT leads to spatial filtering. The stress distributions at the waveguide surface are smoother (leading to low-pass spatial filtering of wavenumbers) and of lower amplitude than those at the top surface of the MPT.
Other similar examples of excellent agreement of the two very different methods have been computed with different parameters (material properties, layer thicknesses, source shape, excitation frequency) but are not shown here for concision. Overall, they give us a great confidence in the ability of the present semi-analytical approach to quantitatively predict the complex wave phenomena in the MPT layered structure.

4. Application to a realistic MPT configuration
The model to transfer distributions of stress from the top surface of a MPT to the surface of a waveguide being validated, it is now possible to chain the electromagneto-elastic model of sources in the magnetostrictive patch with a model of elastic wave radiation in a guide.
MPT are often used for their ability to generate and to be sensitive to shear horizontal modes in plate-like structures (or torsional modes in tubes). Therefore, such a case was chosen to illustrate how the overall modelling approach applies.

Characteristics of the coil geometry are shown on Fig. 10 and Table 2 gives the value of parameters used to define it. The spacing between two consecutive wires is equal to 20 *mm* for an excitation frequency of 80 *kHz*, corresponding to half the wavelength of the (non-dispersive) SH0 mode one wants to radiate preferentially. The value of 40 *mm* for the wavelength was obtained from the dispersion curves shown on Fig. 11 for a 3-*mm*-thick aluminium plate.
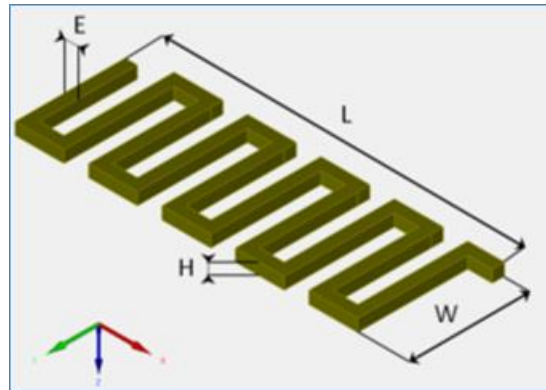

Figure 10. A meander-coil (as defined in CIVA [2])

Table 2. Parameters of the meander coil

E (*mm*)	L (*mm*)	H (*mm*)	W (*mm*)
2	120	2	60

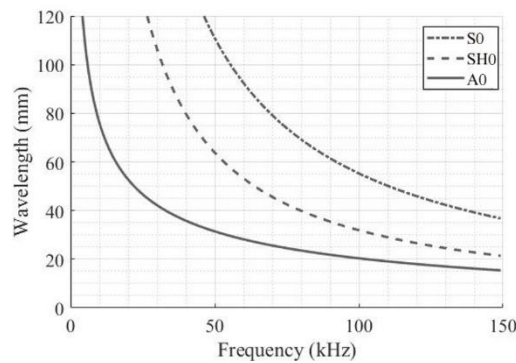This means that for this coil, $L = 3\lambda$.

Figure 11. Dispersion curve for a traction free $3.0mm$ thick Aluminium plate. As the wavelength is plotted, the curve for the SH0 mode is a simple hyperbola.

First, the EMAT model of electromagneto-elastic transduction is used to compute all the dynamic sources. These sources are transformed into equivalent surface stress distributions at the top surface of the MPT. Then, Thomson-Haskell calculation is used to transfer these distributions to the surface of the waveguide. Finally, in this section, these distributions are inputted in a simulation tool for predicting GW radiation in plate-like structures [8]. The ability to predict the radiation characteristics of a given MPT constitutes a very useful mean to optimize MPT design for a given application.

4.1. Dynamic electromagneto-elastic sources
The magnetostrictive strip is made of nickel and is glued (epoxy) to a waveguide made of aluminium. The computation of the induced electromagnetic field in nickel is performed with CIVA [2]. Electric and magnetic properties of Nickel given by Table 3, lead to a skin depth of $19.2\mu m$ at 80 *kHz*.

Table 3. Electric and magnetic properties of nickel	
μ_r	600
$\sigma \ (S.m^{-1})$	14.3×10^6

So, no current is induced in the aluminium plate, considering the thickness of the strip is of 0.2 *mm*, that is, 10 times larger than the skin-depth. The resulting dynamic magnetic flux at a depth equal to a tenth of skin depth is shown on Fig. 12 (components normalized relatively to $\|H_{dx}\|$).
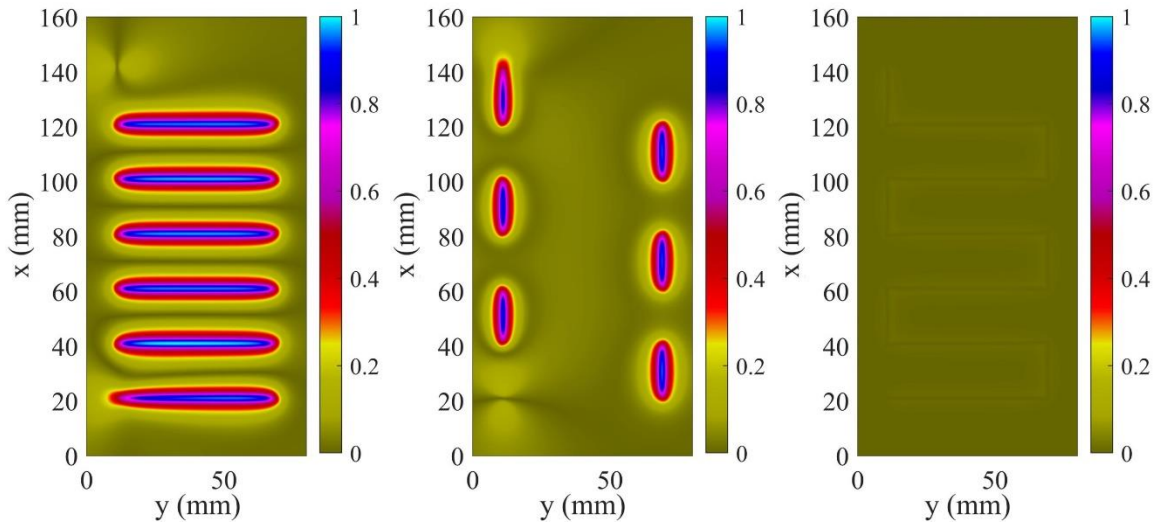

Figure 12. Dynamic magnetic flux: Left: $\|H_{dx}\|$, middle: $\|H_{dy}\|$, right: $\|H_{dz}\|$.

The static magnetic field is supposed to be uniform in the direction $\vec{y}$ and its amplitude is equal 1.2 *kA/m*. The magnetostriction curve (strain *vs.* magnetic field) for nickel is shown on Fig. 13.
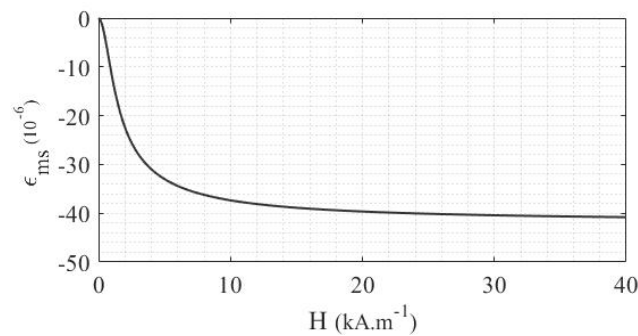

Figure 13. Quasi-static magnetostriction curve for nickel (strain dependency on magnetic field).

The EMAT model combined with the transformation of bulk dynamic sources into equivalent surface stresses computes the distributions of equivalent surface stress from all the electromagneto-elastic phenomena, magnetostrictive strain being predominant in this case. All the contributions are summed up and shown on Fig. 14.
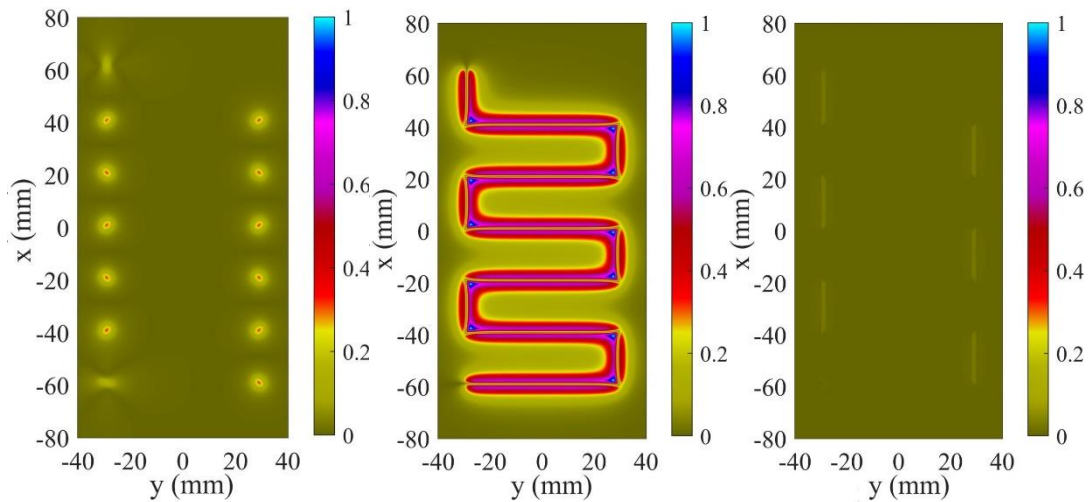
Figure 14. Stress distributions at the surface of the patch. From left to right: $\|\sigma_{xz}\|, \|\sigma_{yz}\|, \|\sigma_{zz}\|$

Given these surface stress distributions, the Thomson-Haskell model presented above allows us to predict the equivalent surface stress distributions at the surface of the aluminium waveguide, shown in Fig. 15. Characteristics of the media of the MPT configuration are given in Table 4.

Table 4. Material properties and thickness of layers used

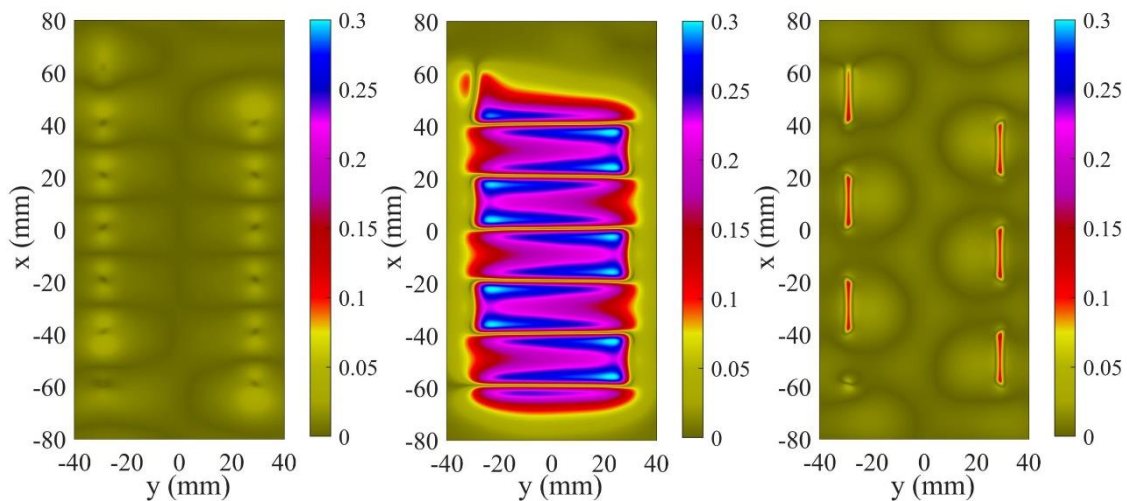|	$\lambda\,(GPa)$	$\mu\,(GPa)$	$\rho\,(kg.dm^{-3})$	$h\,(mm)$
Nickel	136.4	83.6	8.9	0.20
Epoxy	1.27	0.597	1.17	0.20
Aluminum	56.29	26.492	2.6	3.0

Figure 15. Stress distributions at the surface of the waveguide. From left to right: $\|\sigma_{xz}\|, \|\sigma_{yz}\|, \|\sigma_{zz}\|$

The overall transmission through the MPT layers – that accounts for the series of reflections at and transmissions through each interface – results in a smoothing effect of sharp variations of stress at the top surface. Normal stress component is however less affected than the other two components. The absolute amplitude used to scale stress maps at the guide surface in Fig. 15 is 3 times lower than that used to scale stress maps at the top surface of the MPT in Fig. 13. The ratio of transverse stress over normal stress at the surface of the MPT is higher than that at the guide surface as a result of this smoothing effect, normal stress component being less affected.

4.2. GW field computation.

The distributions of stress at the guide surface are now taken as being the source terms of a GW field computation. The aim of computing the field radiated by this complex source is to check that the MPT, designed as described at the beginning of the section, actually radiates preferentially the *SH*0 mode as expected. Such a computation is typical of what can be done thanks to the simulation to quantify the mode selectivity of the MPT.

Various tools are being developed at CEA to make this computation possible: a time-domain FE code [8] and a semi-analytic model (the so-called modal pencil method [8]). The second tool was chosen as it allows us to compute separately the various guided modes radiated into the waveguide.

The norm of particle displacement radiated by the MPT considered herein is mapped on Fig. 16, considering separately the *SH*0 mode (left) and the *S*0 mode (right). The colour bars are chosen to fit the full dynamic of the mode of highest amplitude, namely, the *SH*0 mode. They are scaled to this highest value. For the *S*0 map, the colour bar is taken to be a tenth of that of *SH*0. This shows that the maximum amplitude for *S*0 radiation is more than 10 times lower than that of the *SH*0 mode. The amplitude of *A*0 radiation that is also radiated is so low that it has not been shown.
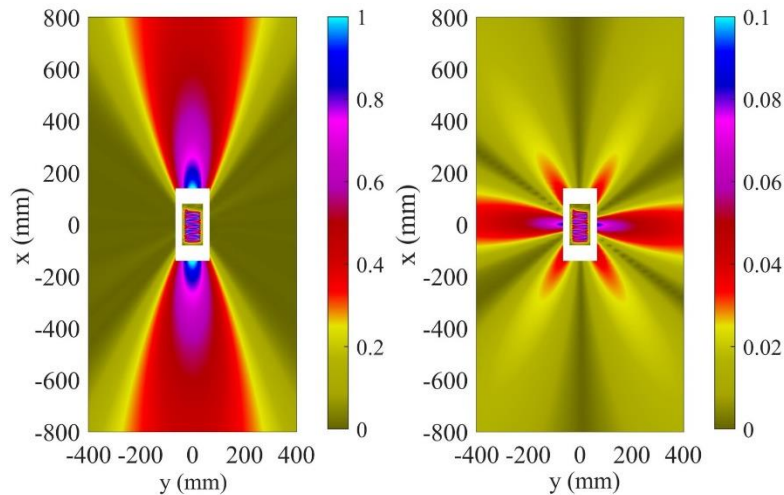

Figure 16. Modal radiation by the MPT given by the norm of particle displacement.
Left: $\|u_{SH0}\|$, right: $\|u_{S0}\|$

The *SH*0 wave field can be described as consisting of two (almost) symmetrical lobes that are highly directive in the *y*-direction. The two lobes are not perfectly symmetrical relatively to the (*x*, *z*) plane as the coil that has been defined does not possess this symmetry.

The *S*0 wave field is of far lower amplitude. However, the radiation of *S*0 waves in the *x*-direction in the form of two lobes cannot be ignored and could probably be source of false alarms in some configurations where these contributions could be scattered by some features of the waveguide.

5. Discussions and future work

Magnetostrictive patch transducers are often described as transducers similar to electro-magneto-acoustic transducers. If there are many papers in the literature (as reviewed in [7]) where the simulation of their behaviour has been studied, most of them make use of multi-physics FE simulations to study the influence of such or such parameter on wave fields MPT radiate.

Here, a semi-analytical model has been derived to adapt a model of EMAT source in ferromagnetic media to the case of MPT. The proposed model relies on local computation of wave propagation within the multi-layered patch structure using a method derived from the Thomson-Haskell method. It results in the prediction of the source of elastic waves the patch generates, given by three distributions of surface

stress at the surface of the piece where the MPT is glued. The method for transferring source terms from the patch surface to the guide surface appears to be both stable and accurate including in cases of complex sources.

Existing validated semi-analytical models [3, 4, 6, 8, 11, 12] were chained so that the modal GW field radiated by a MPT is predicted, given the intensity of current in a coil. The overall model allows one to very efficiently study the influence of the (numerous) parameters to be taken into account when designing a MPT for a given application.

To go further, experimental validations will be conducted to reinforce our confidence that the overall modelling approach is accurate and can be used for optimally design patches to be used in non-destructive evaluation or structural health monitoring methods.

In the present paper, guided wave propagation was considered only in plate-like structures. However, the same methodology can be easily adapted to other geometries of waveguide (tubes). Similarly, it can be adapted to methods relying on the radiation of bulk elastic waves, using the surface source of stress as the input of a model of radiation by arbitrary source [14].

6. Appendix A

This appendix details the expressions of matrices D, E appearing in Sec. 2. All the variables are defined in Table A1.

$$D_m = \begin{bmatrix} k_x g_P & k_x/g_P & k_x k_z^S g_S & -k_x k_z^S/g_S & k_y g_S & k_y/g_S \\ k_y g_P & k_y/g_P & k_y k_z^S g_S & -k_y k_z^S/g_S & -k_x g_S & -k_x/g_S \\ k_z^P g_p & -k_z^P/g_P & -(k_x^2+k_y^2)g_S & -(k_x^2+k_y^2)/g_S & 0 & 0 \\ -2i\mu k_x k_z^P g_p & \dfrac{2i\mu k_x k_z^P}{g_P} & -i\rho k_x B g_S & -i\rho k_x B/g_S & -i\mu k_y k_z^S g_S & \dfrac{i\mu k_y k_z^S}{g_S} \\ -2i\mu k_y k_z^P g_p & \dfrac{2i\mu k_y k_z^P}{g_P} & -i\rho k_y B \, g_S & -i\rho k_y B/g_S & i\mu k_x k_z^S g_S & -\dfrac{i\mu k_x k_z^S}{g_S} \\ -i\rho B g_p & -i\rho B/g_P & 2\mu i k_z^S (k_x^2+k_y^2)g_S & -\dfrac{2\mu i k_z^S(k_x^2+k_y^2)}{g_S} & 0 & 0 \end{bmatrix}$$

$$E_m^{-1} = \begin{bmatrix} \dfrac{k_x}{k_S^2} & \dfrac{k_y}{k_S^2} & \dfrac{B}{2k_z^P.\omega^2} & \dfrac{ik_x}{2\mu k_z^P k_S^2} & \dfrac{ik_y}{2\mu k_z^P k_S^2} & \dfrac{i}{2\mu.k_S^2} \\ \dfrac{k_x}{k_S^2} & \dfrac{k_y}{k_S^2} & \dfrac{-B}{2k_z^P.\omega^2} & \dfrac{-ik_x}{2\mu k_z^P k_S^2} & \dfrac{-ik_y}{2\mu k_z^P k_S^2} & \dfrac{i}{2\mu k_S^2} \\ \dfrac{k_x B}{2\omega^2 k_z^S(k_x^2+k_y^2)} & \dfrac{k_y B}{2\omega^2 k_z^S(k_x^2+k_y^2)} & \dfrac{-1}{k_S^2} & \dfrac{ik_x}{2\mu k_S^2(k_x^2+k_y^2)} & \dfrac{ik_y}{2\mu k_S^2(k_x^2+k_y^2)} & -\dfrac{i}{2\mu.k_z^S.k_S^2} \\ \dfrac{-k_x B}{2\omega^2 k_z^S(k_x^2+k_y^2)} & \dfrac{-k_y B}{2\omega^2 k_z^S(k_x^2+k_y^2)} & \dfrac{-1}{k_S^2} & \dfrac{ik_x}{2\mu k_S^2(k_x^2+k_y^2)} & \dfrac{ik_y}{2\mu k_S^2(k_x^2+k_y^2)} & \dfrac{i}{2\mu k_z^S k_S^2} \\ \dfrac{k_y}{2(k_x^2+k_y^2)} & \dfrac{-k_x}{2(k_x^2+k_y^2)} & 0 & \dfrac{ik_y}{2\mu k_S^2(k_x^2+k_y^2)} & \dfrac{-ik_x}{2\mu k_S^2(k_x^2+k_y^2)} & 0 \\ \dfrac{k_y}{2(k_x^2+k_y^2)} & \dfrac{-k_x}{2(k_x^2+k_y^2)} & 0 & \dfrac{-ik_y}{2\mu k_z^S(k_x^2+k_y^2)} & \dfrac{ik_x}{2\mu k_z^S(k_x^2+k_y^2)} & 0 \end{bmatrix}$$

Table A1. Variable glossary

	Description	Parameter/Equation
ω	angular frequency	model input
k_x	wavenumber in the direction $\vec{x}$	model input
k_y	wavenumber in the direction $\vec{y}$	model input

h	height separating two parallel planes	model parameter
μ	Lamé coefficient	material parameter
λ	Lamé coefficient	material parameter
ρ	density	material parameter
k^S	wavenumber of a shear plane-wave	$k^S = \sqrt{\omega^2/v_S^2}$
k_z^S	wavenumber of a shear plane-wave in the direction $\vec{z}$	$k_z^S = \sqrt{\omega^2/v_S^2 - k_x^2 - k_y^2}$
k_z^P	wavenumber of a pressure plane-wave in the direction $\vec{z}$	$k_z^P = \sqrt{\omega^2/v_P^2 - k_x^2 - k_y^2}$
g_s	propagator of shear plane-wave along z	$g_s = e^{-ik_z^S h}$
g_p	propagator of pressure plane-wave along z	$g_P = e^{-ik_z^P h}$
B	simplification variable	$B = \omega^2 - 2\mu(k_x^2 + k_y^2)/\rho$
v_S	shear wave speed	$v_S = \sqrt{\mu/\rho}$
v_p	pressure wave speed	$v_p = \sqrt{(\lambda + 2\mu)/\rho}$

Expressions of matrices in the case of normal incidence:

$$D_{m,S}^0(h) = \begin{bmatrix} k_S g_S(h) & -k_S/g_S(h) \\ i\rho\omega^2 g_S(h) & i\rho\omega^2/g_S(h) \end{bmatrix} \qquad D_{m,P}^0(h) = \begin{bmatrix} k_P g_P(h) & -k_P/g_P(h) \\ i\rho\omega^2 g_P(h) & i\rho\omega^2/g_P(h) \end{bmatrix}$$

$$[E_{m,S}^0]^{-1} = \frac{1}{\omega^2} \begin{bmatrix} \omega^2/(2k_S) & -i/(2\rho) \\ -\omega^2/(2k_S) & -i/(2\rho) \end{bmatrix} \qquad [E_{m,P}^0]^{-1} \frac{1}{\omega^2} \begin{bmatrix} \omega^2/(2k_P) & -i/(2\rho) \\ -\omega^2/(2k_P) & -i/(2\rho) \end{bmatrix}$$

7. References

[1]   Mitra M and Gopalakrishnan S 2016 *Smart Mater. Struct.* **25** 053001
[2]   Information on CIVA tool for guided wave testing: http://www.extende.com/guided-wave-testing-with-civa
[3]   Clausse B, Lhémery A and Walaszek H 2017 *J. Phys.: Conf. Ser.* **797** 012004
[4]   Clausse B 2018 *Modelling of electromagneto-acoustic transducers (EMAT) for the non-destructive testing of ferromagnetic media* PhD dissertation (Université Paris-Saclay, 2018SACLAX011) (in French)
[5]   Seher M and Nagy P 2016 *NDT&E Int.* **84** 1
[6]   Clausse B and Lhémery A 2016 *Wave Motion* **60** 135
[7]   Seung H M and Kim Y Y 2016 *NDT&E Int.* **80** 6
[8]   Barras J, Lhémery A and Impériale A 2020 *Ultrasonics* **103** 106078
[9]   Impériale A and Demaldent E 2019 *Int. J. Numer. Meth. Engng.* **119** 964
[10]   Thomson W T 1950 *J. Appl. Phys.* **21** 89
[11]   Haskell N A 1953 *Bull. Seismol. Soc. Am.* **43** 17
[12]   Dunkin J W 1965 *Bull. Seismol. Soc. Am.* **55** 335
[13]   Daniel L, Hubert O, Buiron N and Billardon R 2008 *J. Mech. Phys. Solids* **56** 1018
[14]   Lhémery A 1994 *J. Acoust. Soc. Am.* **96** 3776